Minimization of Attrition and Breakage in an Airlift Crystallizer

ARTICLE *in* INDUSTRIAL & ENGINEERING CHEMISTRY RESEARCH · JULY 2012

Impact Factor: 2.59 · DOI: 10.1021/ie300432w

6 AUTHORS, INCLUDING:

Anamaria Soare
Delft University of Technology
3 PUBLICATIONS **22** CITATIONS
SEE PROFILE

Richard Lakerveld
The Hong Kong University of Science and Tec…
27 PUBLICATIONS **203** CITATIONS
SEE PROFILE

Andrzej Stankiewicz
Delft University of Technology
74 PUBLICATIONS **1,384** CITATIONS
SEE PROFILE

Herman J. M. Kramer
Delft University of Technology
145 PUBLICATIONS **1,864** CITATIONS
SEE PROFILE

I&EC research
Industrial & Engineering Chemistry Research

Article

pubs.acs.org/IECR

Minimization of Attrition and Breakage in an Airlift Crystallizer

Anamaria Soare,* Richard Lakerveld, Jurjen van Royen, Giorgia Zocchi, Andrzej I. Stankiewicz, and Herman J. M. Kramer

Intensified Reaction and Separation Systems, Delft University of Technology, 2628 CA Delft, The Netherlands

Supporting Information

ABSTRACT: Minimization of secondary nucleation by attrition in industrial crystallizers is a major challenge. In this work, a novel airlift crystallizer has been designed, constructed, and experimentally tested aiming at the reduction of attrition by using air for mixing instead of a stirrer or a circulation pump. It is experimentally demonstrated that in this crystallizer ideal growth, i.e., growth of crystals without any nucleation, can be approached up to a seeding load of 0.5% and crystal size of up to 600 μm. Attrition is considerably decreased in an airlift crystallizer compared to conventional impeller-mixed crystallizers. This air-mixed crystallizer enables the production of crystals of high quality and offers a large flexibility of the final crystal size by manipulating the air flow rate and the sparger design. Comparison of different designs showed a large effect of a gas disengagement zone on the performance of the crystallizer, especially when large crystals were desired. The disengagement zone allows high circulation velocities and thus good mixing without entrainment of the gas bubbles in the downcomer, approaching a uniform suspension of the crystals.

1. INTRODUCTION

Crystallization is a widely used separation and production formation technology for a variety of chemical, biological, and food products. Crystallization has the advantage that typically a high-purity product can be obtained in one processing step, at a relatively low level of energy consumption and mild process conditions.

A key challenge is to improve in the design phase the control over the physical phenomena dominating the process performance and product quality.[1−3] The control over each of these individual physical phenomena is not possible in present industrial crystallizers, because these phenomena are strongly interconnected.

Crystal growth is a key phenomenon in any design of a crystallization process. In order to optimize crystal growth without compromising on the width of the crystal size distribution, it is desirable[2] to include dedicated growth compartments in the design of future crystallizers in which sufficient mixing is provided and shear forces acting on particles are minimized, so reducing secondary nucleation.

Most of the industrial crystallizers are designed to minimize the supersaturation gradients and use impellers or pumping devices to achieve mixing and suspension of the crystals, which leads to strong mechanical interaction between the crystals and the crystallizer hardware and consequently to enhanced levels of attrition. In fluidized-bed or suspension crystallizers, such mechanical contacts are not present, leading to the possibility of growing crystals of large sizes. However, the operation of this type of crystallizer is quite complicated and for an existing design there is little flexibility in terms of product capacity and product quality. In addition, due to the high crystal concentration in the fluidized bed, particle−particle collisions can enhance the secondary nucleation rate in the crystallizer.

In this paper, a promising alternative candidate for a compartment dedicated to growth, an airlift crystallizer, is designed and experimentally tested. This paper is an extension of our previous work,[2,3] in which the feasibility of a bubble column to suppress attrition was tested. It was concluded that the hydrodynamics have to be improved to be able to increase the mass fraction of a crystal population without nucleation.

The airlift crystallizer consists of a bubble column (riser) in which the liquid phase is mixed by an air flow injected through a sparger and an outer cylinder (downcomer) in which no gas is injected. In this crystallizer, there is no need for a stirrer as circulation flow is induced by the density difference between the riser and the downcomer.

Airlift columns are frequently encountered for applications in biotechnology.[4] The low shear forces present in air-mixed devices help to prevent damage to microorganisms.[5,6] Haut et al.[7] developed a model to describe the precipitation of sodium bicarbonate in an industrial bubble column, which was partially equipped with an airlift. The solid phase is described by a mass fraction in equilibrium with the liquid phase. The gas phase both supports the reaction by introducing carbon dioxide into the system and facilitates mixing. Saberi et al.[8] developed an empirical crystallization model for the same system by fitting power laws to data from an industrial bubble column crystallizer. Bao et al.[9] studied an integrated bioreaction−crystallization process using two external loop airlift columns, which were used for continuous production and crystallization of calcium gluconate. The process was optimized for productivity and loss of catalyst, which was found to be at least comparable to the traditional batch process. In a subsequent paper, Bao et al.[10] focused on the crystallization kinetics in the airlift column. The depletion of calcium gluconate was compared between a stirred crystallizer and airlift crystallizer. In both crystallizers only crystal growth was

Received: February 17, 2012
Revised: June 19, 2012
Accepted: July 23, 2012
Published: July 23, 2012

observed and no influence of stirrer speed or air flow was observed, which indicated that the crystallization kinetics for the studied system were not influenced by hydrodynamic conditions and that air did not interact with crystals such that the kinetics were influenced.

The circulation velocity, and consequently mixing, in the airlift crystallizer is strongly influenced by the air flow rate, the properties of the liquid in contact with air, and the design of the sparger. Typically, three main hydrodynamic regimes can be identified.[5] In regime I, the air immediately escapes from the top of the crystallizer and there is no carryover of air from riser to downcomer. In regime II, part of the air bubbles are entrained into the downcomer, but there is no air carryover into the riser from the bottom of the downcomer. Regime III is characterized by circulation of air between downcomer and riser. In practice, no clear transitions between the regimes can be observed, but rather a gradual transition. Mixing and liquid circulation have an important influence on the crystallization behavior. Optimal liquid circulation prevents stagnant zones, which can easily trigger primary nucleation, and prevents settling of crystals.

The aim of the presented work is to develop and analyze specific gas-mixed-crystallization equipment in which the crystal growth can be isolated from attrition. First, a simple bubble column was used to investigate the feasibility of an air-mixed crystallizer to minimize secondary nucleation. Second, an airlift crystallizer was designed to improve on the observed lack of axial mixing in the bubble column. The airlift crystallizer was designed based on experience from the literature on the design of bioreactors[5] and on experimental data obtained from the bubble column.

Results will be presented for batch crystallization experiments, which show that in the airlift crystallizer ideal conditions can be obtained for crystal growth, minimizing secondary nucleation. As will be shown in the paper, this air based crystallizer design enables the production of crystals of high quality, but also maintains a large flexibility manipulating the operation parameters. Therefore, the paper also discusses in detail the optimization of the crystallizer design, the seeding procedure, and the operating conditions during the batch experiments in which the required product quality and the often desired flexibility are obtained.

This paper is organized as follows. Section 2 describes the design of the airlift crystallizer. Section 3 introduces the experimental approach involving the bubble column and airlift crystallizer. Section 4 includes the results of the crystallization experiments in terms of obtained crystal size distributions (CSDs). Finally, section 5 discusses the performance of the airlift crystallizer compared to the performance of stirred crystallizers, and section 6 concludes the paper.

2. DESIGN OF AN AIRLIFT CRYSTALLIZER

2.1. Base Case Design. An airlift crystallizer is designed using a simplified flow model to determine the key design variables, which are the riser area, aspect ratio, and superficial gas velocity in the riser. The aim is to design an airlift crystallizer with optimal performance, which requires maximization of the liquid circulation velocity for an ammonium sulfate−water system by designing optimal equipment dimensions for typical operating conditions. The purpose of the airlift crystallizer is to isolate crystal growth by providing sufficient mixing and minimal secondary nucleation. The mixing is optimized by maximizing the liquid circulation velocity and the secondary nucleation is minimized by preventing regions of high shear forces, which is ensured by imposing an upper constraint on the circulation velocity. Therefore, the model needs to be capable of predicting the liquid circulation velocity as a function of system properties, equipment dimensions, and operating conditions.

The design of the crystallizer is based on a hydrodynamic model developed by Heijnen et al.[5] in which constant properties of the liquid and solid phases are assumed. Hydrodynamic conditions such as the solid fraction and particle swarm velocity change during the course of crystallization. An estimate of the dominating gas phase regime in an internal airlift crystallizer has to be made for design purposes. The gas phase regime is strongly correlated to the scale of operation. On the laboratory scale, regime I is typically present, while on the industrial scale regime III is more likely due to a larger attainable liquid circulation flow. Heijnen et al.[5] estimate that regime III is only possible if the effective height of the column divided by a friction factor (K_f) is larger than approximately 0.1 m, and therefore for a small scale operation (height H = 1 m) regime III is only possible if the flow reversal is very smooth (K_f = 5) and not hindered for example by the sparger. The intended design for the lab-scale airlift crystallizer is expected to be at the boundary of regimes I and II. It is assumed for design purposes that regime I is prevailing. The design is based on an ammonium sulfate−water system. A high solid concentration and monodispersed CSD with a large mean (700 μm) are chosen, which represent challenging conditions for the airlift crystallizer occurring at the end of a batch or during steady state in continuous flow mode.

The particle slip velocity (v_{PS}) is estimated using the model of Barnea and Mizrahi,[11] which was derived for a two-phase system. It is an empirical model, which takes into account the particle size, solid fraction, density difference between liquid and solid phases, and liquid viscosity. For estimation of the gas holdup in the riser, it is assumed that the riser behaves as a bubble column.

The following empirical model estimates the gas holdup as a function of superficial gas velocity:

$$\varepsilon_{GR} = \alpha\left(\frac{v_{Gs}}{m}\right)^{\beta} \tag{1}$$

where ε_{GR} is the volumetric gas holdup, v_{Gs} is the superficial gas velocity, m is the ratio of the riser area to total area, α and β are system-dependent parameters. For an air−water−ammonium sulfate system, the gas holdup is significantly larger than that for an air−water system, which is caused by smaller air bubbles in the column due to different liquid properties (surface tension, ionic strength, viscosity, etc.). Experimental data from a 3 L bubble column setup (section 3.1) is used to obtain the parameters α = 1.74 and β = 0.84. Typically for an air−water system the values of the parameters found are α = 0.6 and β = 0.7.[12]

The difference between the parameter values shows the importance of adjusting the design of airlift systems that are typical for applications in biotechnology to account for different properties that are typical for crystallization systems (e.g., high salt concentration).

Table 1 summarizes the values for system properties, fixed operating conditions, and design variables. The resulting model has three parameters, 20 variables, and 13 model equations (for details of the model, see Heijnen et al.[5]). The sensitivity of the

Table 1. System Properties, Operating Conditions for Design, and Remaining Degrees of Freedom for Design of an Airlift Crystallizer for an Ammonium Sulfate−Water System

variable		value	comment
	System Properties		
ρ_L	liquid density, kg/m^3	1248	saturated solution at 50 °C[13]
ρ_S	solid density, kg/m^3	1768	at 50 °C[13]
g	gravity acceleration, m/s^2	9.81	
	Operating Conditions		
v_{PS}	particle swarm velocity, m/s (L_M = 700 μm)	0.030	from Barnea and Mizrahi[11]
ε_{GD}	gas fraction downcomer	0	gas phase regime I
ε_S	average solid fraction	0.20	
V_T	total volume, m^3	0.010	
	Design Variables		
m	ratio of riser area to total area		
R	aspect ratio (effective height over total diameter)		
v_{GS}	superficial gas velocity		

average liquid velocity as a function of the design variables is investigated using the model to optimize mixing. The average liquid circulation velocity is a weighted average between the velocity in the riser and the velocity in the downcomer taking into account the areas of the riser and the downcomer. The equipment dimensions are characterized by the ratio of the riser area to total area and by the aspect ratio of the column (m and R, respectively) and operating conditions are determined by the superficial gas velocity (v_{Gs}). Figure 1 shows the dependence of

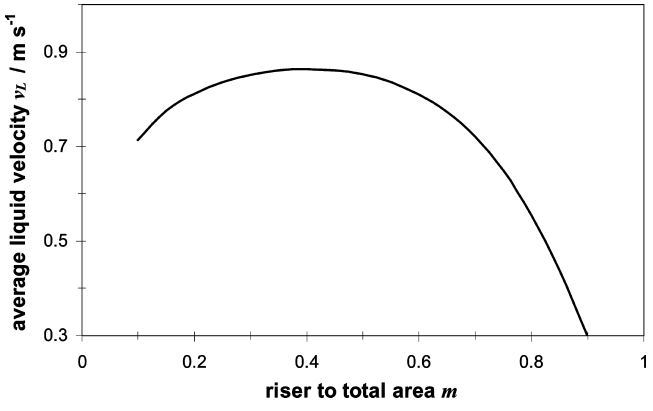

Figure 1. Average liquid velocity as a function of the ratio of riser area to total area (m) with fixed aspect ratio (R = 10) and superficial gas velocity (v_{Gs} = 0.04 m/s).

the liquid circulation velocity on the ratio of the riser area to total area. A maximum value of the liquid velocity can be found just below a value of m = 0.5. A small riser area results in a large gas holdup in the riser (superficial gas velocity is based on total column area) and therefore larger circulation velocity. The friction due to flow reversal at the bottom becomes large for a small or large riser area. Therefore, an optimum can be found at an intermediate riser area. Figure 2 shows the dependence of the liquid circulation velocity on the aspect ratio. The liquid circulation velocity shows an optimum around R = 65. A large aspect ratio results in a large hydrostatic pressure difference and thus a large driving force for circulation at the expense of

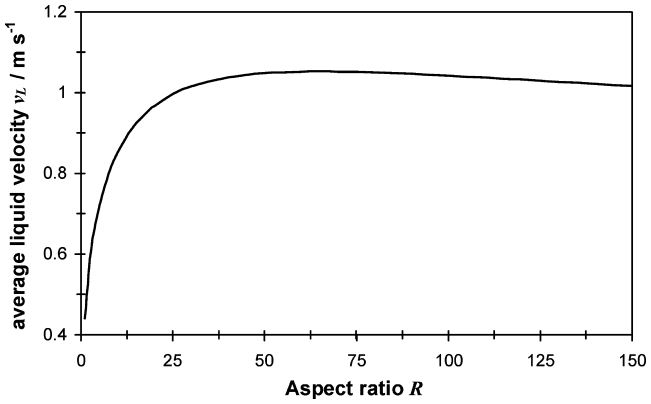

Figure 2. Average liquid velocity as a function of the aspect ratio (R) with fixed ratio of riser to total area (m = 0.5) and superficial gas velocity (v_{Gs} = 0.04 m/s).

increased friction at the wall. Note that the optimum is rather flat and only a slight improvement in liquid circulation velocity can be expected at the expense of increased equipment costs.

Figure 3 illustrates the dependence of the liquid circulation velocity on the superficial gas velocity. The system exhibits state

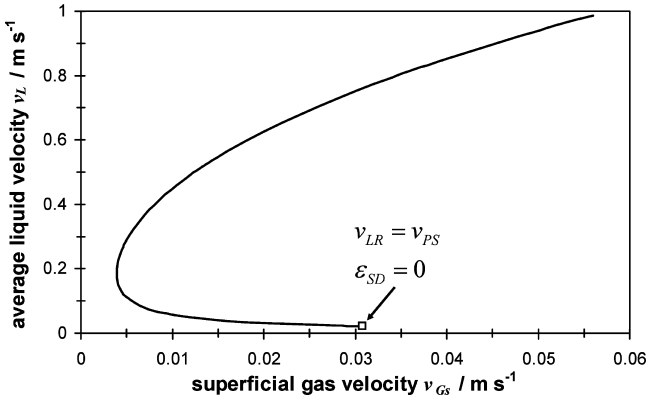

Figure 3. Average liquid velocity as a function of the superficial gas velocity (v_{Gs}) with fixed ratio of riser to total area (m = 0.5) and aspect ratio (R = 10).

multiplicity, and local parametrization is used to track the turning point. Upon increasing the superficial gas velocity, several regions with different steady-state behavior can be identified. At low superficial gas velocity (v_{Gs} < 0.004) no stable steady state can be found. The driving force is insufficient to keep the crystals in suspension. By increasing the gas velocity and upon crossing the turning point, three different stationary states can be identified: a stable upper branch, an unstable middle branch, and a stable lower branch in the infeasible domain (not shown).

1. The stable upper branch has a high liquid circulation velocity. The solids are distributed over the riser and downcomer, which causes a large density difference between the riser and downcomer for circulation and entrainment of the crystals. In case all solids accumulate in the riser (ε_{SR} = 0.4), suspension of the crystals is lost. Operation on this branch poses a risk as fluctuations in operating conditions can result in loss of suspension.

2. The stationary states on the middle branch are unstable (saddle points). Any deviation from these points will move the system to one of the stable steady states.

dx.doi.org/10.1021/ie300432w | Ind. Eng. Chem. Res. 2012, 51, 10895−10909

3. The lower stable branch can be found in the physical infeasible domain for the studied system.

Upon further increasing the superficial gas velocity, the number of stationary states changes to one (stable upper branch) due to the occurrence of a feasibility limit. At the feasibility limit, all solids are accumulated in the riser ($\varepsilon_{SR} = 0.4$, $\varepsilon_{SD} = 0$) and the superficial gas velocity is sufficient to generate an upward liquid velocity in the riser that is equal to the particle swarm velocity. For any larger superficial gas velocity, the liquid velocity in the riser is larger than the particle swarm velocity independent of the distribution of solids over the riser and downcomer. This region is a preferred region of operation as suspension of solids can always be achieved.

An iterative scheme is used to determine the optimal design variables as illustrated in Figure 4. The design is based on

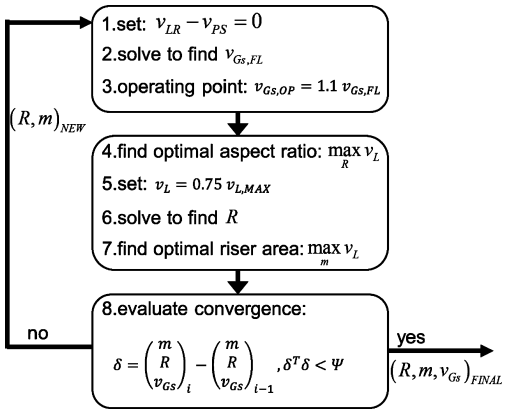

Figure 4. Algorithm for the determination of the equipment dimensions (m, R) and the typical superficial gas velocity (v_{Gs}) for airlift crystallizer. $v_{Gs,FL}$ is the minimum superficial gas velocity at which all the solids are fluidized, $v_{Gs,OP}$ is the operating superficial gas velocity, and δ represents the vector with residues for each iteration.

operation in the region without state multiplicity. The aspect ratio is fixed at a smaller value compared to the optimum (based on 75% of the average liquid velocity at the optimal aspect ratio), because the increase in average liquid velocity is small toward the optimum at the expense of increased equipment costs. The values for the design variables are given in Table 2. The found optimal riser area is smaller than half the

Table 2. Optimal Values of Design Variables for Experimental Airlift Crystallizer

variable		value
m	ratio of riser area to total area	0.41
R	aspect ratio	9.2
v_{Gs}	default superficial gas velocity, m/s	0.035

total area. The calculated values for riser area and aspect ratio are the basis for construction of an experimental setup involving a 10.0 L airlift crystallizer as described in section 3.2.

2.2. Extension Design. An air disengagement room has been designed to potentially improve the separation of the gas and liquid phases at the top of the airlift crystallizer. The airlift crystallizer can be operated with or without the air disengagement room to investigate the benefits that can be obtained by extending the design.

The airlift crystallizer has been designed by assuming operation in flow regime I, but this might not always be achieved for certain systems or operating conditions. Operation outside flow regime I increases the gas fraction in the downcomer and thus reduces the driving force for circulation. The desired operating regime is I, but at a small scale the regimes are close and the uncertainty of the bubble sizes in saturated salt solutions makes this even more problematic. Large crystals could settle at the bottom due to insufficient liquid circulation if the system is operated close to flow regime III (circulating bubbles) already for low superficial gas velocities. In this scenario, fewer crystals would be present at the top part of the column and nucleation could be induced. The mixing would certainly not be optimized, which has consequences on the final crystal size that can be obtained.

To improve the operational flexibility by the ability to increase the circulation velocity and at the same time maintaining operation in regime I, a degasification zone at the top of the crystallizer was designed with the aim of decreasing the gas holdup by lowering the velocity of the liquid.

In order to allow for air to escape the crystallizer instead of recirculating into the downcomer and riser, the liquid velocity in the disengagement room should be smaller than the bubble swarm velocity. The air bubble swarm velocity in water varies between 0.14 and 0.2 m/s.[5] From experiments it can be concluded that the bubble swarm velocity in an ammonium sulfate−water solution is smaller as the bubble size is smaller than in water. The ratio of the riser to the disengagement room is calculated by fixing the condition that the liquid circulation velocity should be smaller than 0.1 m/s. Using the continuity equation and taking into account the velocity in the riser (calculated using the model explained in section 2.1) and the maximum desired velocity in the disengagement room, the ratio of the riser to the disengagement room cross-sectional areas can be calculated. Figure 5 illustrates the dependence of the liquid

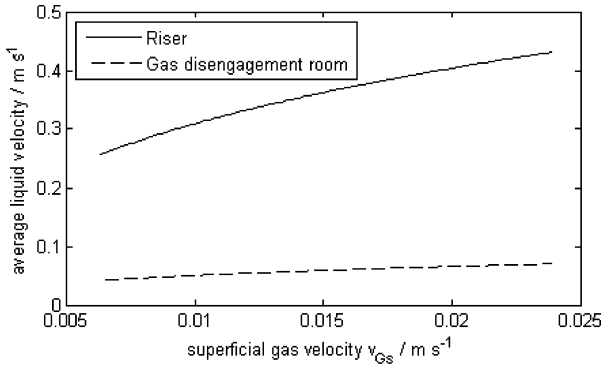

Figure 5. Average liquid velocity in the riser and in the gas disengagement room as a function of the superficial gas velocity (v_{Gs}) with fixed ratio of riser to downcomer area ($m = 0.41$) and fixed ratio of riser to disengagement room area ($m_2 = 0.14$).

circulation velocity in the riser and in the gas disengagement room on the superficial gas velocity. It can be observed that the average liquid velocity in the disengagement room is 5 times smaller than the velocity in the riser. The height of the room should be small enough to avoid stagnant zones, but large enough to allow for air bubbles to escape. An average residence time of 3 s for the bubbles is considered to be sufficient. A smooth transition from the smaller diameter of the airlift external column to the bigger diameter of the disengagement

room is necessary in order to minimize the crystal−wall collisions and to avoid settling of crystals. The values of the design parameters of the air disengagement room are given in Table 3.

Table 3. Values of Design Variables for the Air Disengagement Room Placed on Top of the Airlift Crystallizer

variable		value
m_2	ratio of riser to disengagement room area	0.14
R	aspect ratio of the height with respect to the diameter	2.25

The experimental setup extended with an air disengagement room increases the total volume of the system from 10.0 to 18.0 L. A detailed description of the experimental setup involving the airlift system discussed in this section is presented in section 3.

3. MATERIALS AND METHODS

In this section the experimental setups and procedures used are explained in detail.

3.1. Bubble Column. The bubble column, Figure 6, was made out of Perspex (poly(methyl methacrylate)) and had an internal diameter of 7.0 cm and height of 1.0 m (liquid holdup 3.4 L). Pressurized air (8 bar, 0.002 kg of water/kg of dry air) reduced to 1.2 bar at room temperature was introduced by a gas sparger (perforated plate, d_{hole} = 800 μm). The superficial gas velocity was flow controlled, and the inlet pressure was measured by a digital manometer. The temperature was measured at six different locations by resistance thermometers (Pt-100). The gas phase was partially condensed using two cooling spirals to collect the vaporized water. For a description of the experiments on the bubble column, see section 4.1.

3.2. Airlift Crystallizer. The airlift crystallizer was experimentally tested in two different configurations. The first configuration does not involve a gas disengagement section and is referred to as configuration AL-I. The second configuration involves the airlift crystallizer including a gas disengagement zone and is referred to as configuration AL-II.

3.2.1. Airlift Crystallizer without Gas Disengagement (AL-I). A schematic drawing of the experimental setup involving a 10.0 L airlift crystallizer without a gas disengagement section is given in Figure 7. The airlift crystallizer was made from stainless steel and consisted of an inner draft tube and external jacketed wall. The jacket was connected to a thermostatic bath (Ecoline Staredition RE310, Lauda), which was connected to an external temperature sensor (Pt-100) to control the temperature inside the airlift crystallizer. The jacket contained channels in a spiral shape to prevent shortcutting of the liquid from the thermostatic bath and to cool the contents of the airlift crystallizer reasonably quickly. Note that evaporation of the

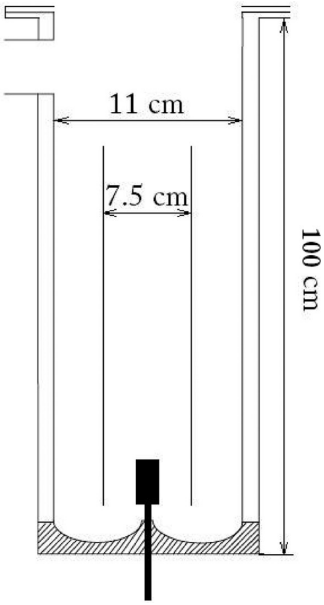

Figure 7. Schematic drawing of the airlift crystallizer without gas disengagement zone (AL-I).

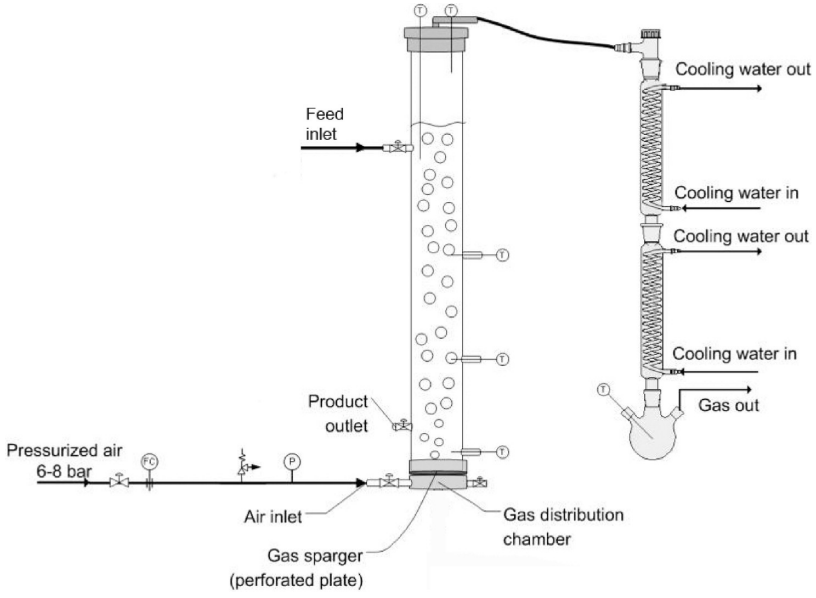

Figure 6. Schematic representation experimental setup involving a bubble column.[3]

solvent also contributed to cooling. The calculated ratio of the riser area to total area and the aspect ratio (Table 2) were the basis for design. The height of the downcomer was chosen to be 1.0 m. The dimensions of the airlift crystallizer are indicated in the drawing (Figure 7). A viewing glass was installed to observe the presence of air bubbles in the downcomer and to inspect the survival of the introduced seed crystals. The bottom part was shaped such that the cross-sectional area of the flow remained constant during flow reversal. The interior of the crystallizer was honed to minimize friction with the wall. Two different types of gas sparger could be inserted inside the riser. The first sparger, referred to as sparger A, was commercially available and was made of porous metal with pores of 0.1 mm diameter and a surface area of 46 cm^2 (Mott sparger 2306-A04-6-A00-100-AB). The second sparger, referred to as sparger B, was a smooth stainless steel pipe with 15 holes of 1 mm diameter. The spargers were connected to pressurized air (8 bar, room temperature, 0.002 kg of water/kg of dry air) with two parallel flow controllers (0−500 and 0−3000 $L_n\ h^{-1}$, where L_n is normal liters) to deliver a controllable gas flow rate over a broad range. The temperature was measured at four different locations (bottom and top of both riser and downcomer) to detect possible temperature gradients in the crystallizer.

A typical batch experiment started with the preparation of a saturated solution. A jacketed vessel was filled with demineralized water and an excess of ammonium sulfate (commercial grade, DSM, The Netherlands). The temperature of the stirred vessel was controlled at 65 °C using a thermostatic bath (Huber CC-231) with an external temperature probe (Pt-100). The solution was prepared at least 1 day before the experiment to ensure equilibrium. The column was preheated at 75 °C at the start of the experiment and the column was rinsed once with saturated solution to remove traces of water. The air flow was fixed at 300 L/h during filling to prevent liquid from entering the gas inlet. The solution was maintained approximately 20 min at elevated temperature to ensure complete dissolution of all crystals, after which a temperature program was started. At the end of the batch, the CSD of the produced crystals was measured with a laser diffraction instrument (S3500 particle size analyzer, Microtrac). Ultrasound was applied to break possible agglomerates. Microscopic pictures were used to observe crystal shape and to qualitatively validate the CSD measurements with laser diffraction.

In the airlift crystallizer, supersaturation was generated by simultaneous cooling and evaporation. A temperature profile was developed, which aimed to match the generation of supersaturation with the consumption of supersaturation. The applied temperature−time profile was described by

$$T(t) = T_0 + at + bt^2 + ct^3 \tag{2}$$

The coefficients of eq 2 were fixed by solving the following optimization problem:

$$\min_{a,b,c}\left[\int (G(t) - G^{REF})^2\, dt\right] \tag{3}$$

$$G^{REF} = \frac{L_{MAX} - L_{SEED}}{t_{END}} \tag{4}$$

$$T(t_{END}) = 25\ °C \tag{5}$$

$$-0.5 \le \frac{dT}{dt} \le 0.5 \tag{6}$$

$$20\ °C < T(t) < 80\ °C \tag{7}$$

where L_{MAX} is the crystal size in case of no nucleation (so-called ideal growth).

The objective function from eq 3 is similar to the one used in our prior work.[14] The crystal growth rate (G) as a function of relative supersaturation (σ) is assumed to be independent of crystal length and is described by a simple power law function as

$$G = k_G \sigma^{\gamma} \tag{8}$$

where k_G is the growth rate constant and γ is the exponential factor of the growth rate. The relative supersaturation is described by the following relation:

$$\sigma = \frac{w - w_{SAT}}{w_{SAT}} \tag{9}$$

where w is the actual concentration and w_{SAT} is the saturation concentration.

For an ammonium the sulfate−water system, k_G is 7.5×10^{-5} m/s, γ is 1, and the solubility (mass fraction) is given by[3]

$$w_{SAT} = 0.41179 + (9.121 \times 10^{-4})T \tag{10}$$

The seeding point was corrected for the evaporation during start-up, which was determined from separate experiments in which the level was monitored for several gas velocities. The optimization was implemented in gPROMS (Process Systems Enterprise Ltd.), and a typical example of a temperature profile that resulted from the optimization is given in Figure 8. The temperature rose in the beginning to increase solubility, and the temperature gradient hit the constrained value at the end of the batch.

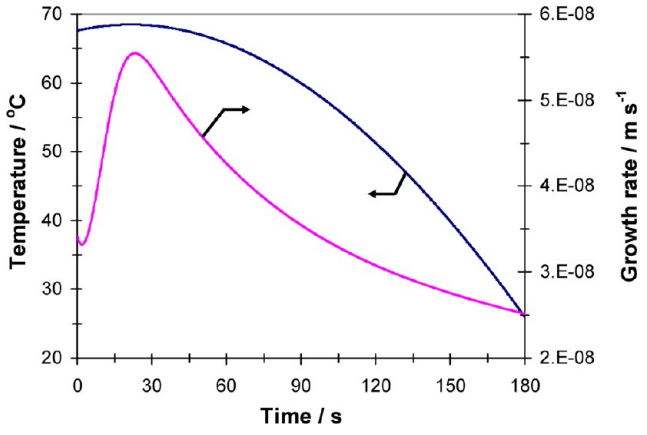

Figure 8. Example of a temperature profile with fixed batch time in airlift crystallizer, which matches supersaturation generation with consumption considering simultaneous cooling and evaporation for an ammonium sulfate−water system with seed crystals (10 g, 115 μm) used for start-up.

Ideal growth is defined as a situation where the number of crystals remains constant during the batch. In the case of ideal growth, the following equation can be used to calculate the crystal size.[15]

dx.doi.org/10.1021/ie300432w | Ind. Eng. Chem. Res. 2012, 51, 10895−10909

$$\frac{L_{MAX}}{L_{SEED}} = \left(\frac{C_S + 1}{C_S}\right)^{1/3} \quad (11)$$

in which L_{SEED} is the seed volume based mean size and C_S is the seed load defined as the seed mass (W_{SEED}) divided by the crystalline mass produced ($W_{crystals,theoretical}$):

$$C_S = \frac{W_{SEED}}{W_{crystals,theoretical}} \quad (12)$$

Equation 11 is valid when the number of crystals remains constant, the crystal shape does not change, and there is no residual supersaturation.[15] Furthermore, the width of the CSD should be sufficiently small as the method uses the volume based mean size to estimate the total number of crystals. At each CSD measurement the crystal size in the case of ideal growth can be estimated by calculating the theoretical yield at the time of measurement and by applying eq 11. It gives the mean crystal size that is achieved if all of the crystal mass produced so far has been deposited on the seeds. Note that this approach does not take into account changes in supersaturation. The levels of supersaturation are in general low for an ammonium sulfate−water system, which justifies this assumption.

A 100 mL jacketed seeding vessel was used to prepare seed crystals for start-up. A saturated solution was placed into the seeding vessel, which was closed to prevent evaporation and stirred with a magnetic bar. The temperature was controlled with a temperature probe (Pt-100) and heating plate (RCT Basic, IKA Laboratory Equipment). The temperature was increased to 5 °C above saturation for at least 30 min before it was controlled at the saturated value to ensure complete dissolution of all crystals. The seed crystals were ground crystals (commercial grade ammonium sulfate, DSM, The Netherlands) and classified by sieving (fraction 90−100 μm). The seeds were preheated in an oven and suspended in the saturated solution in the seeding vessel before insertion into the airlift crystallizer to remove (crystalline) dust adhering to the surface and to heal the crystal lattice. Figure 9 shows the development of the crystal median size for different stirring speeds as a function of time (distribution width remained constant). It can be seen that the median size increased as a function of time and a steady state was not reached within 2 h. It was decided to insert the seeds after a residence time of 1 h in the seeding vessel (seed median size of approximately 110 μm) assuming that the crystal facets healed sufficiently to allow for crystal growth upon introduction in the airlift crystallizer.

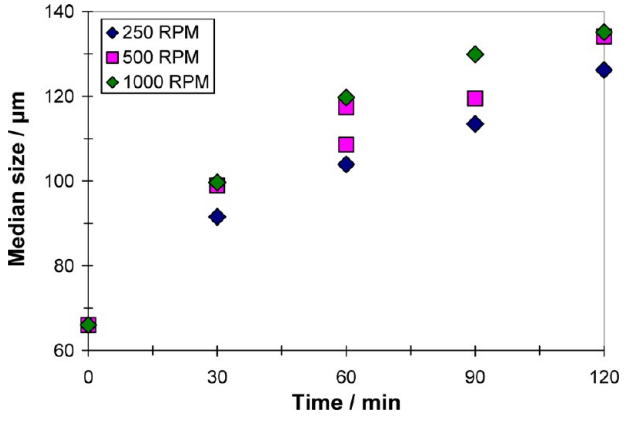

Figure 9. Development of crystal median size of seeds suspended in seeding vessel (20 wt %, 90−100 μm sieve fraction, in saturated solution at 65 °C) as a function of time for various stirrer speeds (magnetic bar).

An overview of the conducted experiments is given in Table S1 in the Supporting Information. Experiments 1 and 2 were done to investigate the influence of ammonium sulfate on the hydrodynamics. In addition, experiments 9 and 11 were used to compare the influence of a different sparger on the hydrodynamics. Experiments 3−8 aimed to investigate the growth of seeded populations with different masses and different supersaturations in the airlift crystallizer at the seeding point. Sparger A with fine pores and a rough surface (Mott) was used for these experiments. Experiments 10−18 were done to investigate the growth of various seed populations with sparger B (smooth surface and larger pores). An experiment in which the crystal population was harvested halfway during the batch (experiment 19) was done to investigate the development of the crystal size distribution during the batch. Finally, one experiment (20) with a larger seed size (270 μm) was done to investigate the potential of the system to attain a larger final crystal size.

3.2.2. Airlift Crystallizer with Gas Disengagement Section (AL-II). A schematic drawing of the 18.0 L airlift crystallizer extended with a gas disengagement section is given in Figure 10. All the experiments conducted in the 18.0 L crystallizer were performed by cooling a 60 °C saturated solution to 25 °C. The method to prepare the seeds was simplified by inserting the crystals directly into the crystallizer. An online camera (PIA 524, MTS Particle Technology, Germany) was used to inspect the survival and the evolution of the introduced seeds, which initially were kept at constant temperature for 30 min to allow for healing of the crystal lattice. The temperature profile during the experiments can be seen in Figure 11.

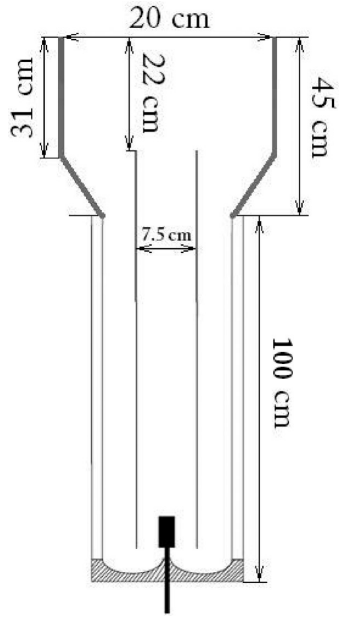

Figure 10. Schematic drawing of the airlift crystallizer extended with a gas disengagement section.

Initially, the solution was kept at 65 °C for 20 min to ensure that the solution was clear. After this period, the solution was cooled to 61.5 °C, which was the seeding temperature. The

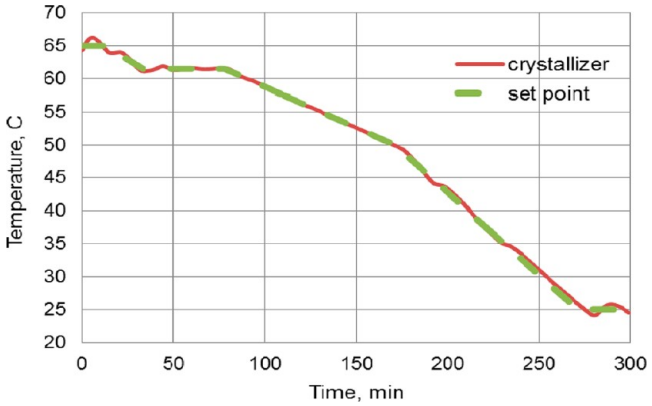

Figure 11. Typical temperature profile during the experiment. The temperature inside the crystallizer is measured inside the gas disengagement section.

solution was kept at this temperature for 15 min to stabilize the temperature, after which the seeding took place. After the healing period, at constant temperature, the solution was cooled to 25 °C in two steps. First, a cooling rate of 0.125 °C/min was applied, followed by a cooling rate of 0.25 °C/min.

Figure 12 shows images of the development of seed crystals as a function of time from two typical experiments (21 and 24 from Table S2 in the Supporting Information). Figure 12a,d shows the seeds just after insertion, at 61.5 °C. Figure 12b,e shows the seed crystals after 25 min of the healing time. It can be observed that the shape of the crystals changed to an orthorhombic shape. The final crystal products are pictured in Figure 12c,f. The size of the crystals increased in time and the shape remained orthorhombic without rounded faces, indicating no dissolution and no attrition. Note that the crystals seen in Figure 12f are bigger compared to those seen in Figure 12c, because the amount of seeds added was smaller in the former case.

A mean size of the seed crystals of 125 μm after the healing period was found via separate experiments. The experiments with both 7 and 40 g of seeds gave nicely faceted crystals. These experiments verified the reproducibility and predictability of the chosen seeding method.

An overview of the conducted experiments with the airlift crystallizer with a gas disengagement section is given in Table S2 in the Supporting Information. Experiments 21−24 were done to investigate the effect of seed mass on the final product. In addition, experiment 25 was conducted without the addition of seeds in order to investigate the effect of primary nucleation. Experiments 23−33 were done to investigate the influence of the air flow rate on the product crystal size distribution for different seeding loads. Experiments 34−39 were used to compare the influence of different spargers on the growth of various seed populations. Experiment 40 was done under the same conditions as experiment 22 in order to determine the variation of the product crystal size distribution.

4. RESULTS

4.1. Bubble Column. The 3 L bubble column was used to measure the gas holdup in a saturated ammonium sulfate−water system in the presence of 5 wt % solids as a function of the superficial gas velocity (Figure 13). The gas holdup was determined by measuring the increase in level of the liquid surface with a calibrated scale after the gas flow rate was turned on. The parameters α and β from eq 1 are fitted to the experimental results and used for the design of the airlift crystallizer to describe the behavior of the riser.

4.2. Airlift Crystallizer without Disengagement Section (AL-I). The influence of the seed load on the product size is first tested. The superficial gas velocity used in the experiments is 1.5 cm/s (535 L/h). For a higher gas flow rate, the volume of the three-phase mixture becomes higher than the volume of the crystallizer. The median sizes obtained in the seeded batch experiments are depicted in Figure 14 as a function of seed load. For both spargers (A and B), no dependency of the final median size on seed load is found. In the case of a small seed load (C_S < 3.0%), the experimentally found median size is smaller compared to ideal growth, which indicates an increase in the number of crystals. For higher seed loads, the experimentally measured final median size is equal to ideal growth or even higher. A larger final median size compared to ideal growth can be the result of agglomeration or ineffective seeding, for example, due to dissolution or settling.

The results obtained with sparger B (Figure 14b) show a behavior similar to those obtained with sparger A (Figure 14a). In both cases the size of the crystals appeared to be independent of the seed load. In the experiments with sparger B, the product size was approximately 100 μm larger, which is most likely the effect of the improved liquid circulation velocity.

To investigate the deviation from ideal growth more closely, an experiment has been done in which the crystals are collected at half the normal batch time (experiment 19, Table S1 in the Supporting Information). A comparison of the measured median size with ideal growth is given in Figure 15. It can be seen that the deviation from ideal growth mainly occurs in the second half of the batch. It can be expected that in the first part of the batch the highest levels of supersaturation and, therefore, undesired nucleation would occur. As this is not the case, an alternative explanation has to be found for the deviation from ideal growth in the second half of the batch experiment. Segregation of larger crystals, which are only present in the second half of the batch, could take place. In this way, larger crystals will be trapped at the bottom part of the crystallizer and this region will exhibit low supersaturation due to the large crystal surface area. In the top part of the column, a shortage of crystal surface area would be present, which might induce nucleation. To investigate this hypothesis, an additional experiment has been done with seeds with a median size of 270 μm (experiment 20), which is approximately the value from which a lack of growth is observed. Indeed, no growth of these seeds is observed and a product of similar size is obtained.

The results presented in this section demonstrate the need to improve the hydrodynamics for the tested system. The flow regimes were studied for water and ammonium sulfate in experiments 1, 2, 9, and 11. The airlift crystallizer has been designed by assuming operation in flow regime I, which proves to be a reasonable assumption only for water at low superficial gas velocities up to 1.2 cm/s. The introduction of ammonium sulfate in the system significantly reduces the bubble size, which increases the gas fraction in the downcomer and thus reduces the driving force for circulation. The system operates close to flow regime III already for low superficial gas velocities. Consequently, depending on the size of the crystals, only a fraction of the crystals is circulated in the system and a fluidized bed with crystals of a certain size in the bottom of the column is the result. Improvements are expected in the experiments with the disengagement zone to prevent entrainment of bubbles into the downcomer.

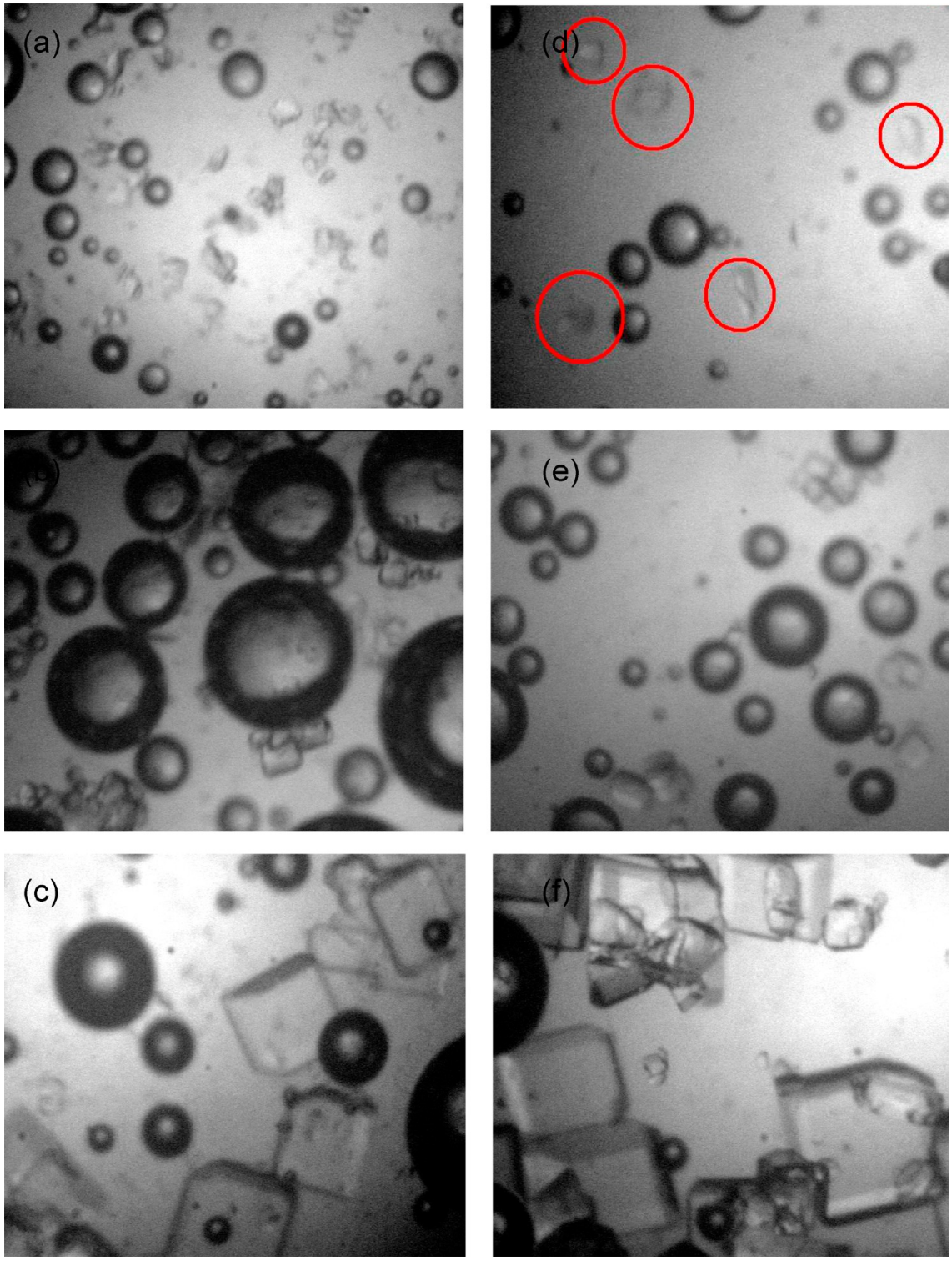

Figure 12. Development of 90−100 μm seed crystals during two typical seeded batch experiments in the extended airlift crystallizer. Seed amounts were 40 g (experiment 24) and 7 g (experiment 21) for (a)−(c) and (d)−(f), respectively. The air flow rate is 400 L/h, and sparger type B was used.

4.3. Airlift Crystallizer with Disengagement Room (AL-II). In the airlift crystallizer equipped with an air disengagement zone, the influence of various process conditions on the product quality was investigated. The first exploited degree of freedom was the amount of seeds inserted into the crystallizer, which is expected to have a direct influence on the final crystal size distribution. The air flow was maintained constant at 400 L/h, and the used sparger was of type B. The results, which are shown in Figure 16, prove that different sizes of product may effectively be reached by varying the amount of seeds inserted into the crystallizer. The CSD obtained with 7 g is wider than the ones obtained with 20, 30, and 40 g of seeds, which could be a consequence of nucleation. The total surface area of the seed crystals is not high enough in this case to consume all the supersaturation by growth, which results in a burst of nucleation. The experiment with 20 g of

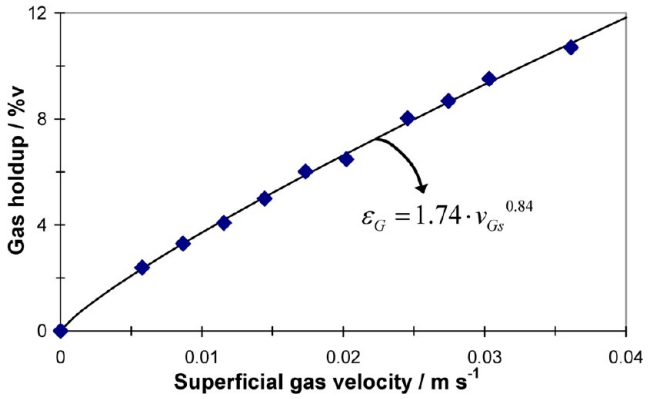

Figure 13. Gas holdup as a function of superficial gas velocity measured in 3 L bubble column for an $(NH_4)_2SO_4$–water system (ε_S = 5 wt %, T = 50 °C, D = 0.07 m).

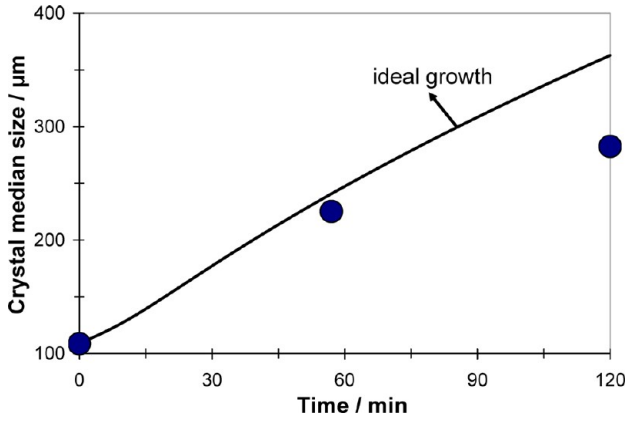

Figure 15. Trend of the median size during the batch. The blue dots are experimentally measured (seeds, experiments 7 and 19). The black line represents the mean size in the case of ideal growth.

seeds had the narrowest CSD. To check the repeatability, this experiment was conducted twice and comparable CSD characteristics (mean size and width) were obtained. Figure 16 shows a long tail in the CSD of the product in the experiment with 30 g and to a lesser extent in that with 40 g of seeds. This broadening of the CSD could be due to nonuniform distribution of the supersaturation, mass transfer limitation, growth rate dispersion, or agglomeration. The agglomeration could take place during the filtration at the end of the experiment, during the measurement, or during the experiment itself. Nonuniform distribution of the supersaturation is not likely to be present, as will be shown in a subsequent paper.

The CSD measurements were always repeated several times to ensure the reproducibility of the measurements. Values for the width of the CSD, which is defined as the ratio of the 90% to the 10% quantile, from the experiments depicted in Figure 16 are given in Table 4. The values are still smaller than the ones obtained in an optimized and controlled 75 L draft tube crystallizer[14] which varied between 2.45 and 3.02.

A series of tests with different air flows was performed in order to investigate how the changes in hydrodynamics influence the final crystal size and shape. Results of experiments at different air flows using seed loads of 7 and 40 g are shown in parts a and b, respectively, of Figure 17.

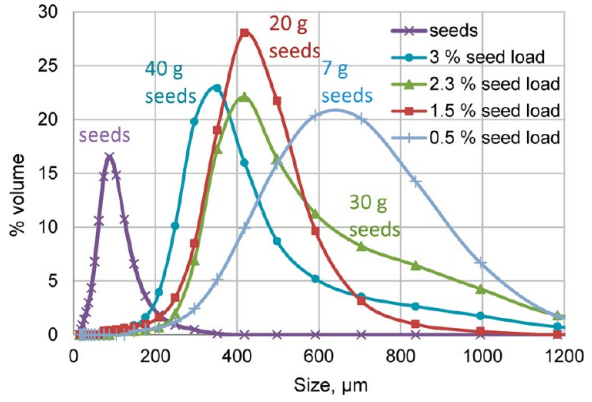

Figure 16. Influence of amount of seeds on the product CSD in airlift crystallizer with gas disengagement zone. The air flow was kept constant at 400 L/h using the sparger of type B (experiments 21–24).

Table 4. CSD Width Function of the Seed Load[a]

seed amount, g	7	20	30	40
X_{90}/X_{10}	2.37	2.17	2.66	2.62

[a] X_{90}/X_{10} of the seeds is 3.33.

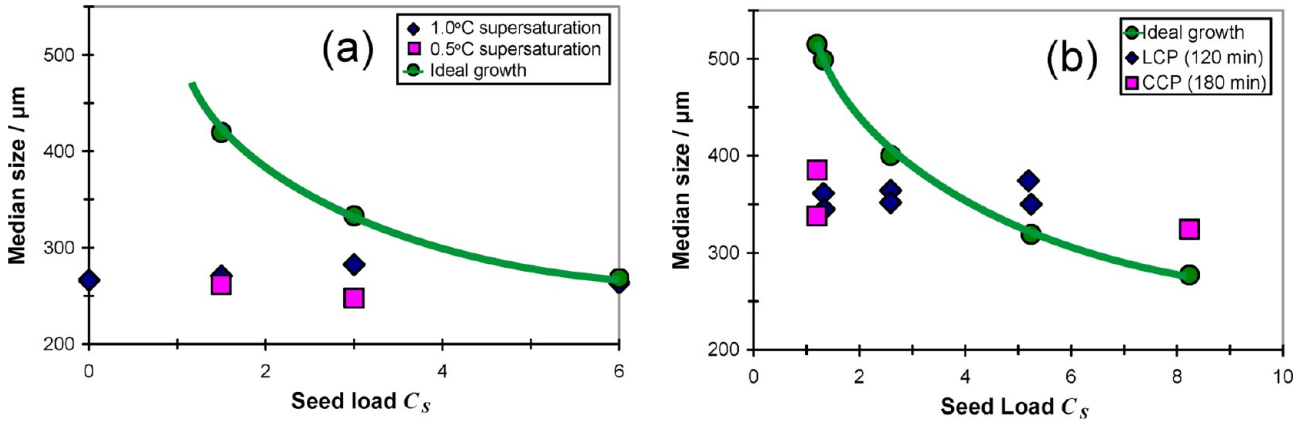

Figure 14. Final median size obtained in seeded batch crystallization in AL-I and under conditions of ideal growth as a function of seed load. (a) Sparger A (experiments 3–8). (b) Sparger B (experiments 10–18). Initial supersaturation in (b) corresponded to a temperature of 2 °C below saturation for all experiments. LCP, linear cooling profile; CCP, calculated cooling profile (as in Figure 8).

dx.doi.org/10.1021/ie300432w | Ind. Eng. Chem. Res. 2012, 51, 10895–10909

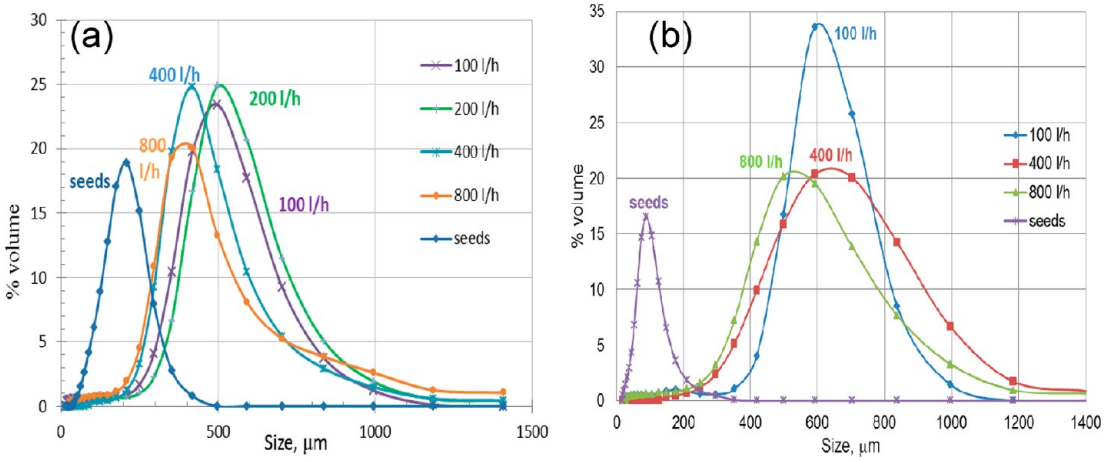

Figure 17. Influence of air flow rate on the product CSD at constant amount of seeds: (a) 40 g of seeds (experiments 24, 30, 31, and 33); (b) 7 g of seeds (experiments 21, 26, and 29).

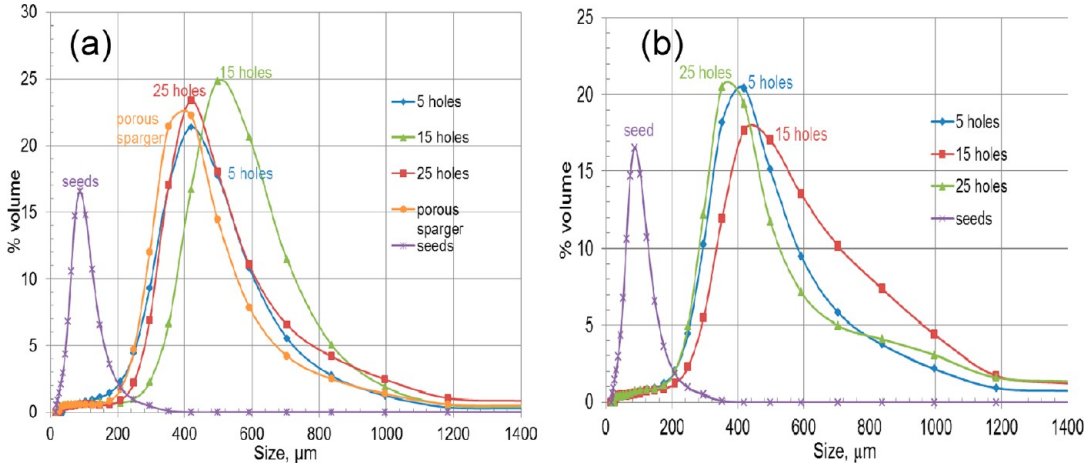

Figure 18. Influence of sparger type on the product CSD: (a) 40 g of seeds and 200 L/h air (experiments 31, 34, 36, and 38); (b) 40 g of seeds and 600 L/h air (experiments 32, 37, and 39).

Figure 17a clearly shows that in the case of 40 g of seed crystals the lower air flows (100 and 200 L/h) result in the largest CSD, whereas at the higher air flows the distribution becomes more bimodal indicating nucleation at the end of the batch. In the experiments with 7 g of seeds (Figure 17b), the low air flows gave larger crystal size and a much narrower CSD. Furthermore, smaller air flows gave better results with respect to the shape and quality. The crystals appear a bit damaged when using high air flow rates, with some of them having inclusions and a shape that changed from orthorhombic into more elongated. This can be a consequence of local evaporation by the air bubbles in the solution increasing the supersaturation. It is possible that the bubbles stick to crystals provoking liquid or air inclusions. From the experiments with varying air flow rates, it could be concluded that the smaller the air flow the better the quality of the crystals.

Next, the influence of the sparger type on the product quality is investigated. Four spargers were tested: the porous metal sparger (A) and three spargers made from a smooth stainless steel pipe with 15 (B), 5 (C), and 25 (D) holes of 1 mm diameter. Experiments were all conducted with 40 g of seeds and at two different air flow rates (200 and 600 L/h). The results of these experiments in terms of CSD are given in Figure 18.

The results obtained with a lower air flow (200 L/h) show that the sparger with 15 holes gave the best results, whereas the other spargers gave comparable results. The experiments with the porous sparger gave the smallest crystals, which might be explained by a different flow regime, which was close to regime III for this experiment, whereas in the experiments with the spargers B, C, and D operation was in regime I.

The experiment with 600 L/h air and the porous sparger (experiment 35) could not be completed due to primary nucleation on the sparger, which caused the air flow to drop to 100 L/h. The results with 600 L/h differ from the result with an air flow rate of 200 L/h. The maximum mean size is still reached with the 15 hole sparger, but the CSD is wider. However, this could be a result of the air flow increase, which gives wider distributions as has been shown previously (Figure 17b).

A 2 L glass airlift crystallizer with the same ratio of the cross-sectional area of the riser and downcomer was constructed to investigate the difference between a sparger with 5, 15, and 25 holes in more detail and to get insights regarding the rules for the sparger design. The bubbles were observed as they left the sparger. Different bubble regimes are depicted in Figure 19 as a function of the sparger type and air flow rate. Figure 19a shows that, at a low flow rate, the air is released from only two out of

dx.doi.org/10.1021/ie300432w | Ind. Eng. Chem. Res. 2012, 51, 10895−10909

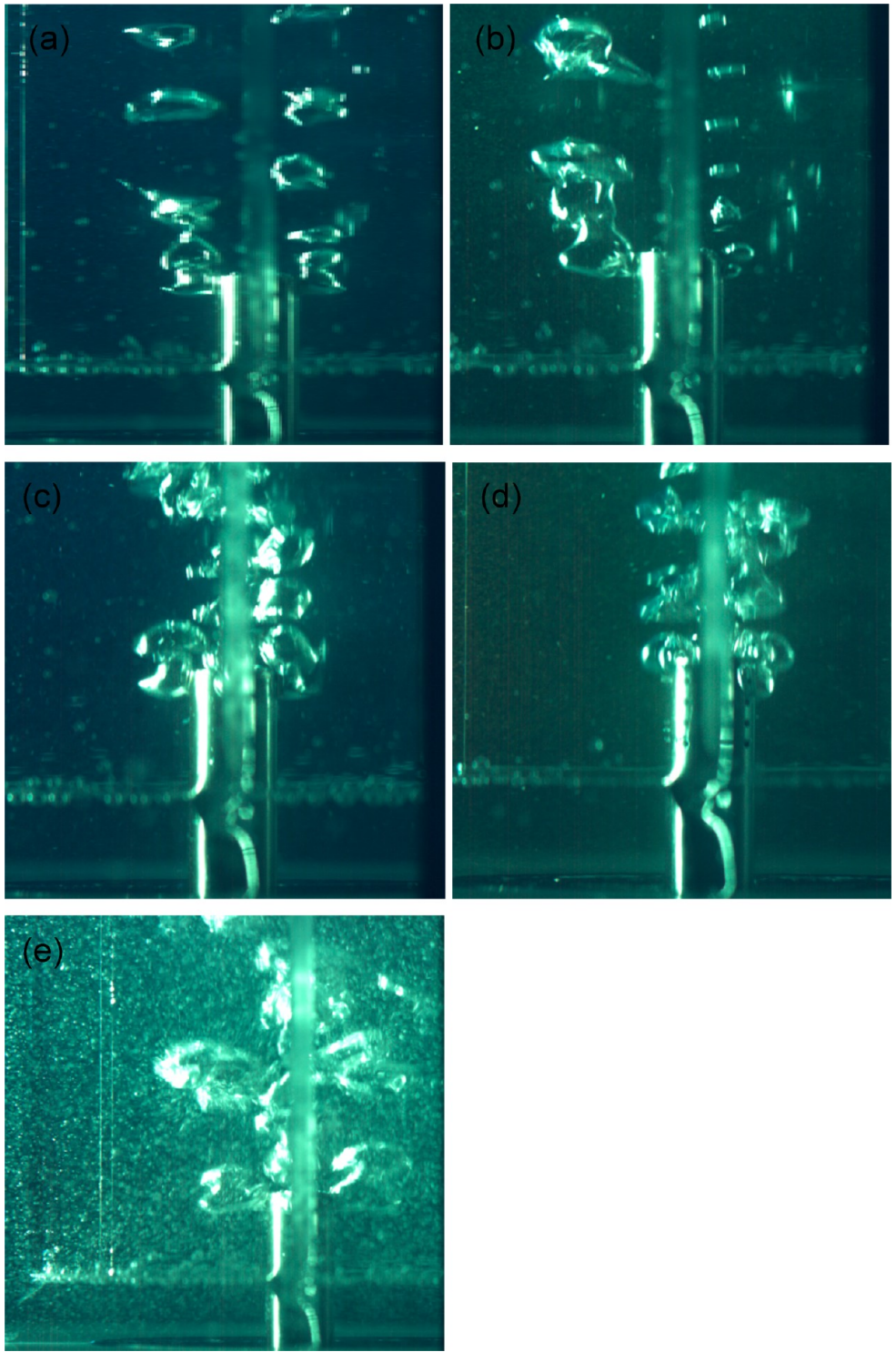

Figure 19. Different operation regimes as a function of sparger type and air flow rate in a 2 L glass airlift crystallizer: (a) 5 holes, 50 L/h; (b) 5 holes, 50 L/h, sparger started to plug; (c) 5 holes, 100 L/h, normal operation; (d) 25 holes, 100 L/h; (e) 5 holes, 300 L/h.

five holes. A similar behavior can be observed in Figure 19d, where the air flow is set at 100 L/h and the sparger has 25 holes. Part of the holes could become plugged when the air flow per hole is too low and the bubbles become smaller and smaller, as seen in Figure 19b (swarms of bubbles at the right). When this happens, the bubble velocity decreases and the gas holdup increases, which causes the hydrodynamic regime to change very rapidly from regime I to regime II. This has two consequences. First, the circulation velocity could decrease and bigger crystals could settle and agglomerate at the bottom of the crystallizer, and second, crystals could have air inclusions due to incorporation of the smallest air bubbles into the crystals. All of these lead to unpredictable and in general undesirable product quality. This can be avoided by designing and using the right sparger for the desired air flow. Normal operation is depicted in Figure 19c, in which the air flow is equally distributed over all holes of the sparger. In Figure 19e the hydrodynamic regime is III even if the sparger is not

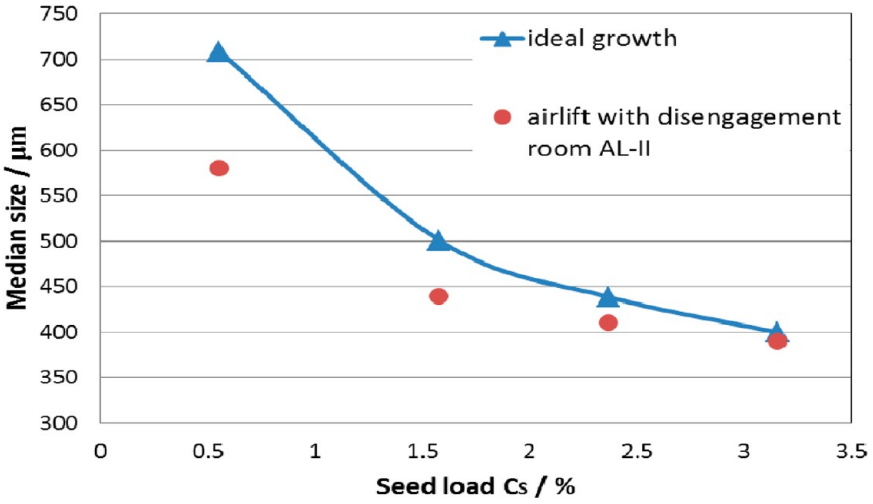

Figure 20. Ideal and real mean sizes at different seed loads in the airlift crystallizer with disengagement room, AL-II.

plugged, which happens because the air flow rate is higher (300 L/h). Note that the 2 L crystallizer has no gas disengagement room.

The performance of the airlift crystallizer is shown in Figure 20 by comparing the median size of crystals obtained in the experiments that are illustrated in Figure 16 to the size in case ideal growth would occur. The airlift crystallizer equipped with a disengagement room shows that crystal growth follows the ideal growth curve reasonably well.

The performance of the airlift crystallizer with a gas disengagement room, AL-II, can be compared also to that of the airlift without a disengagement room, AL-I, to that of the bubble column, and to that of agitated crystallizers with the help of a seeding chart (Figure 21). A seeding chart[16] shows the

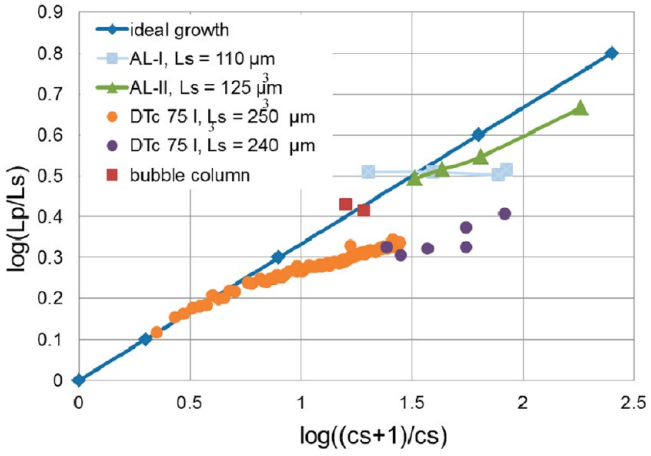

Figure 21. Seed chart showing results from the airlift crystallizer with disengagement room compared to ideal growth line, to bubble column,[3] and to a 75 L draft tube agitated crystallizer.[2,17]

mean size (Lp) as a function of the ratio of seed mass to the total crystal mass produced (cs). A straight line indicates the ideal growth line at which the number of crystals in the batch is equal to the number of seed crystals. The experimental data from the agitated crystallizer have been obtained from a 75 L draft tube (DT) crystallizer as described in prior work.[2,17] The behavior of the 75 L DT crystallizer illustrated in the seed chart compares well to experimental data that can be obtained for the same system in a stirred vessel at a 1 L scale.[18]

5. DISCUSSION

The system properties are of primary interest for the design and scale-up of an airlift crystallizer, because of their effect on the performance and hydrodynamics. Preliminary design calculations can be done, but the effects of the solute and crystal concentration should be taken into account. However, these effects are difficult to predict.

There are a number of ways to manipulate the hydrodynamics, which are most importantly the use of an air disengagement zone, the sparger design, and the air flow rate. Coarse or fine bubble aeration systems can be used as air spargers. The coarse air bubbles are preferred for a number of reasons: (1) they induce higher liquid circulation velocity, (2) they more easily get out on the top of the crystallizer and operation remains in regime I even at higher air flow rates, and (3) they are less likely to induce nucleation compared to fine bubbles. The spargers made from smooth stainless steel still are preferred as they are more effective in preventing clogging. The sparger should be specifically designed for the desired range of air flow rates to avoid clogging.

The optimal air flow rate is determined by several criteria. The air flow rate must be high enough to induce a sufficient liquid circulation velocity to maintain all the crystals in suspension and ensure a homogeneous mixing, while minimizing the gas holdup at the same time. Therefore, the liquid circulation velocity should be a few times higher than the maximum settling velocity of the crystals to ensure that the crystals can be dispersed in the solution once settling accidently has occurred. Time-dependent conditions in which the air flow rate is increased during the batch could be exploited as well. In this way, a smaller air flow rate could be used at the beginning of the batch when the crystals are small and easy to maintain in suspension, which also has the advantage of minimizing the gas holdup and thus the risk of nucleation and inclusions in the crystal lattice. The risk of nucleation due to the air bubbles could be further minimized by eliminating the solvent evaporation into the air by saturating the air with solvent prior to injection into the crystallizer.

If continuous operation is desired, the settling of the crystals of a certain size could be an important advantage as the product

will have a narrow CSD without a tail of big crystals. Also, such a crystallizer operated in continuous mode could be flexible as the size of the product can potentially be controlled by the air flow rate.

As mentioned before, operation in hydrodynamic regime I is preferred. This can be obtained by manipulating the ratio of the cross-sectional areas of the riser and downcomer to lower the liquid velocity in the downcomer and to avoid entrainment of the bubbles. Alternatively, the addition of a gas disengagement zone, in which the liquid velocity is reduced, favors operation in regime I.

The superficial gas velocities used in the experiments performed in this work were relatively low, and the air bubbles were homogeneously distributed in the riser and coalescence was hardly observed. In industrial-scale crystallizers this homogeneous bubbly flow most likely changes into a slug flow which could be an advantage as this would decrease entrainment of the bubbles in the downcomer. The bubble coalescence and breakage at different scales have recently been described using a combined integrated computational fluid dynamics and bubble population balance model. The approach was successfully applied to simulate the gas holdup in gas−liquid stirred tanks at different scales.[19] Regarding the scale-up possibilities, one option is to increase the size of the riser, downcomer, and gas disengagement room, keeping the same hydrodynamic operation regime and same liquid circulation velocities as in the lab-scale setup. Heijnen et al.[5] predict that the scale-up of an airlift crystallizer will lead to operation in regime III. This prediction is valid for airlift reactors without disengagement zones and with riser area fractions between 0.4 and 0.5. Operation in regime I can be maintained by decreasing the riser area and increasing the downcomer area or by using a disengagement room.

An industrial case in which struvite (magnesium ammonium phosphate hexahydrate) is precipitated in an airlift crystallizer has also been studied[20] in order to gain insights regarding an alternative for scale-up of such a crystallizer. This industrial-scale airlift reactor is used to remove phosphate and residual organic matter from a wastewater stream by producing large struvite crystals 2−3 mm long. The crystals are needle shaped and accordingly they are sensitive toward attrition, which can be minimized in air-mixed crystallizers. The airlift crystallizer for struvite has multiple risers and only one downcomer, the height of which is bigger than the height of the risers. The upper part plays the role of a disengagement and classification zone, which serves not only for air disengagement, but also for separation of the crystals. The small and thus light crystals stay in the upper part of the crystallizer and the bigger and heavier crystals settle at the bottom, from where they are harvested.

6. CONCLUSIONS

An airlift crystallizer was designed, constructed, and experimentally tested with the purpose to isolate crystal growth by minimizing attrition and breakage. The results indicate that an airlift crystallizer can be flexible to control the size of the crystalline product by the seed load and the air flow rate.

Comparison of different designs showed the large effect of a gas disengagement zone on the performance of the crystallizer, especially when large crystals are desired. The disengagement zone allows high circulation velocities and thus good mixing without entrainment of the gas bubbles in the downcomer, approaching in this way a uniform suspension of the crystals.

The influence on the final crystal size distribution was investigated for the following three variables: the amount of seeds, the air flow rate, and the type of air sparger. The final crystal size that was experimentally obtained was close to the size calculated under the assumption that only crystal growth occurs, at least up to a seeding mass as low as 0.5 wt % of the final yield. The air flow rate and the sparger geometry influence the hydrodynamics in the crystallizer. The desired flow regime has no gas in the downcomer of the airlift crystallizer. The flow of pressurized air injected in the riser of the crystallizer has an influence on both the liquid circulation velocity and the size of the bubbles. The crystals might settle and agglomerate at the bottom of the crystallizer if the liquid circulation velocity is not high enough, which can trigger primary nucleation in the bulk of the solution. The air flows used in the experiments were varied between 100 and 800 L/h. The low air flows gave larger crystals with narrower CSDs. The influence of the sparger is crucial for the hydrodynamics as the design of the sparger influences the bubble size. In addition, the sparger can act as a template for heterogeneous primary nucleation. In the presented work, a few sparger designs are tested. A sparger with a smooth surface and a limited number of holes gives the best results in terms of avoiding nucleation and attaining an optimum CSD. The number of holes should be adapted to the desired air flow rate.

Woo et al.[21] and Aamir et al.[22,23] managed to effectively turn off nucleation in impeller-mixer crystallizers by having fine control of supersaturation. Although they demonstrated the growth of large crystals by turning off nucleation in impeller-mixer crystallizers, the overall crystal mass growth rate is limited in those approaches by the supersaturation being limited by the presence of the impeller. All of the past approaches of concentration control within a crystallizer to produce large crystals can be extended to the airlift crystallizer that can in principle have higher crystal mass growth rate due to removal of the impeller.

■ ASSOCIATED CONTENT

Ⓢ Supporting Information

An overview of the conducted experiments with the airlift crystallizer with and without gas disengagement section is given in Tables S1 and S2. This material is available free of charge via the Internet at http://pubs.acs.org.

■ AUTHOR INFORMATION

Corresponding Author

*E-mail: a.soare@tudelft.nl.

Notes

The authors declare no competing financial interest.

■ REFERENCES

(1) Menon, A. R.; Pande, A. A.; Kramer, H. J. M.; Jansens, P. J.; Grievink, J. A task-based synthesis approach toward the design of industrial crystallization process units. *Ind. Eng. Chem. Res.* **2007**, *46* (12), 3979−3996.

(2) Lakerveld, R.; Kramer, H. J. M.; Jansens, P. J.; Grievink, J. The application of a task-based concept for the design of innovative industrial crystallizers. *Comput. Chem. Eng.* **2009**, *33* (10), 1692−1700.

(3) Lakerveld, R. Development of a Task-Based Design Approach for Solution Crystallization Processes. Dissertation, Delft University of Technology, Delft, The Netherlands, 2010.

(4) Joshi, J. B.; Ranade, V. V.; Gharat, S. D.; Lele, S. S. Sparged Loop Reactors. *Can. J. Chem. Eng.* **1990**, *68* (5), 705−741.

(5) Heijnen, J. J.; Hols, J.; vanderLans, R. G. J. M.; vanLeeuwen, H. L. J. M.; Mulder, A.; Weltevrede, R. A simple hydrodynamic model for the liquid circulation velocity in a full-scale two- and three-phase internal airlift reactor operating in the gas recirculation regime. *Chem. Eng. Sci.* **1997**, *52* (15), 2527−2540.
(6) Merchuk, J. C. Airlift bioreactors: Review of recent advances. *Can. J. Chem. Eng.* **2003**, *81* (3−4), 324−337.
(7) Haut, B.; Halloin, V.; Cartage, T.; Cockx, A. Production of sodium bicarbonate in industrial bubble columns. *Chem. Eng. Sci.* **2004**, *59* (22−23), 5687−5694.
(8) Saberi, A.; Goharrizi, A. S.; Ghader, S. Precipitation kinetics of sodium bicarbonate in an industrial bubble column crystallizer. *Cryst. Res. Technol.* **2009**, *44* (2), 159−166.
(9) Bao, J.; Koumatsu, K.; Furumoto, K.; Yoshimoto, M.; Fukunaga, K.; Nakao, K. Optimal operation of an integrated bioreaction-crystallization process for continuous production of calcium gluconate using external loop airlift columns. *Chem. Eng. Sci.* **2001**, *56* (21), 6165−6170.
(10) Bao, J.; Koumatsu, K.; Arimatsu, Y.; Furumoto, K.; Yoshimoto, M.; Fukunaga, K.; Nakao, K. A kinetic study on crystallization of calcium gluconate in external loop airlift column and stirred tank for an immobilized glucose oxidase reaction with crystallization. *Biochem. Eng. J.* **2003**, *15* (3), 177−184.
(11) Barnea, E.; Mizrahi, J. A generalized approach to the fluid dynamics of particulate systems: Part 1. General correlation for fluidization and sedimentation in solid multiparticle systems. *Chem. Eng. J.* **1973**, *5* (2), 171−189.
(12) Heijnen, J. J.; Van't Riet, K. Mass transfer, mixing and heat transfer phenomena in low viscosity bubble column reactors. *Chem. Eng. J.* **1984**, *28* (2), B21−B42.
(13) Jager, J. Control of Industrial Crystallizers: The Physical Aspects. Dissertation, Delft University of Technology, Delft, The Netherlands, 1990.
(14) Mesbah, A.; Huesman, A. E. M.; Kramer, H. J. M.; Nagy, Z. K.; Van den Hof, P. M. J. Real-Time Control of a Semi-Industrial Fed-Batch Evaporative Crystallizer Using Different Direct Optimization Strategies. *AIChE J.* **2011**, *57* (6), 1557−1569.
(15) Jagadesh, D.; Kubota, N.; Yokota, M.; Doki, N.; Sato, A. Seeding Effect on Batch Crystallization of Potassium Sulfate under Natural Cooling Mode and a Simple Design Method of Crystallizer. *J. Chem. Eng. Jpn.* **1999**, *32* (4), 514−520.
(16) Jagadesh, D.; Kubota, N.; Yokota, M.; Sato, A.; Tavare, N. S. Large and mono-sized product crystals from natural cooling mode batch crystallizer. *J. Chem. Eng. Jpn.* **1996**, *29* (5), 865−873.
(17) Kalbasenka, A. N.; Spierings, L. C. P.; Huesman, A. E. M.; Kramer, H. J. M. Application of seeding as a process actuator in a model predictive control framework for fed-batch crystallization of ammonium sulphate. *Part. Part. Syst. Charact.* **2007**, *24* (1), 40−48.
(18) Hojjati, H.; Rohani, S. Cooling and seeding effect on supersaturation and final crystal size distribution (CSD) of ammonium sulphate in a batch crystallizer. *Chem. Eng. Process.: Process Intensif.* **2005**, *44* (9), 949−957.
(19) Gimbun, J.; Rielly, C. D.; Nagy, Z. K. Modelling of mass transfer in gas-liquid stirred tanks agitated by Rushton turbine and CD-6 impeller: A scale-up study. *Chem. Eng. Res. Des.* **2009**, *87* (4A), 437−451.
(20) Soare, A.; Kollmann, I. M.; Lakerveld, R.; Kramer, H. J. M.; Abma, W. Modeling of an airlift crystallizer for struvite production. In *BIWIC 2009 16th International Workshop on Industrial Crystallization, Lappeenranta, Finland*; Louhi-Kultanen, M., Hatakka, H., Eds.; Lappeeenranta University of Technology: Lappeenranta, Finland, 2009; pp 371−378.
(21) Woo, X. Y.; Tan, R. B. H.; Braatz, R. D. Precise tailoring of the crystal size distribution by controlled growth and continuous seeding from impinging jet crystallizers. *CrystEngComm* **2011**, *13* (6), 2006−2014.
(22) Aamir, E.; Nagy, Z. K.; Rielly, C. D. Optimal seed recipe design for crystal size distribution control for batch cooling crystallisation processes. *Chem. Eng. Sci.* **2010**, *65* (11), 3602−3614.
(23) Aamir, E.; Nagy, Z. K.; Rielly, C. D. Simulation and Experimental Evaluation of Seed and Supersaturation Control Design Approaches for Crystallisation Processes. *Comput.-Aided Chem. Eng.* **2010**, *28*, 763−768.